Model for inclusion formation in low alloy steel welds

S. S. Babu, S. A. David, J. M. Vitek, K. Mundra, and T. DebRoy

Oxide inclusion formation in low alloy steel welds is described with a model as a function of weld metal composition and process parameters. The model was developed by coupling thermodynamic and kinetic considerations. Thermodynamic calculations considered the effect of the alloying elements and kinetic equations allowed, describing oxide formation during weld cooling. The model showed that weld cooling rate influences the inclusion characteristics and therefore must be taken into consideration. This inclusion model is capable of predicting the composition, size, number density, and oxidation sequence of inclusions and was verified with published data. The inclusion model was coupled with numerical heat transfer and fluid flow models to extend the model to a wide range of welding process conditions.

Dr Babu, Dr David, and Dr Vitek are in the Metals and Ceramics Division, Oak Ridge National Laboratory, Oak Ridge, TN 37831–6095, USA, Dr Mundra is with General Electric, 1 Research Circle, Nisakayuna, NY 12309, USA, and Professor DebRoy is in the Department of Materials Science and Engineering, Penn State University, 212 Steidle Building, University Park, PA 16802, USA. *Manuscript received 1 December 1998; accepted 11 January 1999.*

INTRODUCTION

The relationship between acicular ferrite and improved low alloy steel weld metal properties is well established.[1–4] It is also known that acicular ferrite formation depends on inclusion characteristics, solidification conditions, austenite grain structure, austenite to ferrite transformation kinetics, and weld cooling conditions.[5] There exists extensive research on the effect of these parameters on acicular ferrite formation. However, an integrated weld model that is capable of quantifying all these interactions as a function of welding process parameters (such as welding voltage, current, speed, shielding environment, etc.) and weld metal composition (concentrations of, for example, oxygen, nitrogen, aluminium, titanium, silicon, etc.) is not available. The present paper addresses this need and focuses on the development of a model for inclusion characteristics such as number density, size, composition, oxidation sequence, volume fraction, and concentration of residual deoxidiser elements.

The inclusions that exist in low alloy steel welds are mostly heterogeneous oxides with small amounts of sulphides and nitrides. These inclusions form owing to complex reaction sequences that occur during weld cooling (Fig. 1). In the temperature range 2600–1800 K, deoxidation reactions prevail in liquid steel, i.e. reactions between dissolved oxygen and deoxidiser elements such as aluminium, titanium, silicon, and manganese. During solidification (in the approximate temperature range 1800–1700 K), sulphides may form in addition to oxides. In later stages of weld cooling, in the solid state ($\sim$1700–1000 K), nitrides may form heterogeneously on the pre-existing oxide inclusions.[6] Further cooling below 1000 K leads to solid state decomposition of austenite to different ferrite morphologies. These reactions occur over a specific temperature range and the extent of these reactions depends on kinetics as well as thermodynamics. Therefore, the present work considers both weld metal composition and weld cooling rate.

In earlier studies by other investigators,[7–10] inclusion formation was related to the weld metal composition and the standard free energy of formation of various oxides. In the original work of Kluken and Grong,[7] sequential oxidation in the order Al_2O_3, Ti_2O_3, SiO_2, MnO was assumed. This sequential deoxidation was originally proposed by Bailey and Pargeter.[8] Other researchers have used a similar approach.[9] Later, Bhadeshia and Svensson[10] applied the same method to predict inclusion composition as a function of weld metal composition. However, in all of the above mentioned studies, the effect of actual weld metal composition on oxide formation was ignored. As a result, the sequence of oxidation remained the same regardless of the concentration of alloying element.

To overcome this limitation, Babu *et al.*[11,12] developed a methodology to describe inclusion formation in low alloy steel welds by coupling the thermodynamics of oxide formation with overall transformation kinetics principles. Later, Hsieh *et al.*[13] used ThermoCalc[14] software to describe the complex oxide formation as a function of weld metal composition without considering the kinetics. Koseki *et al.*[15] described inclusion formation in liquid steel, during solidification and in the solid state, by considering multicomponent and multiphase equilibrium thermodynamics. However, they ignored kinetic considerations. Therefore, in these latter two studies,[13,15] the oxidation sequence for a particular weld composition remained the same regardless of the weld metal cooling conditions. This is a serious limitation which reduces the applicability of such models to a wide range of welding conditions.[16] In addition, these models are not capable of predicting the inclusion number density.

However, the earlier work of Babu *et al.*[11] showed that oxidation sequence and inclusion formation depend strongly on the weld metal composition, the reaction temperature, and the weld cooling conditions. Later, Babu *et al.*[12] illustrated some preliminary calculations of inclusion characteristics using the above methodology. The present paper extends the work of Refs. 11 and 12, to describe:

(i) development of an integrated inclusion model that considers the reactions in the liquid steel during weld cooling (2300–1800 K)
(ii) the effect of modified weld cooling conditions on inclusion formation
(iii) the results of integrating the inclusion model with coupled fluid flow and heat transfer models.

INCLUSION MODEL DEVELOPMENT

Although much of the background for the development of this model has been discussed in the previous work,[11,12] the

 ISSN 1362–1718

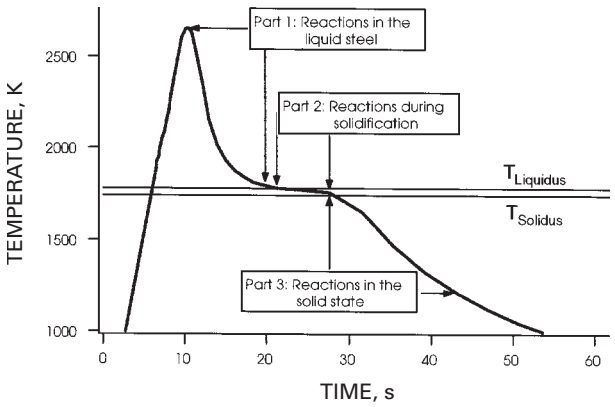

1 Typical weld metal thermal cycle showing different regions of reactions requiring consideration in developing generalised inclusion model

present paper describes the methodologies and specific assumptions used in developing an integrated weld inclusion model. In this model, the formation of simple oxides such as Al_2O_3, Ti_3O_5, Ti_2O_3, TiO_2, TiO, SiO_2, and MnO was considered, as well as formation of AlN and MnS. In addition, one of the complex oxides, $MnO.Al_2O_3$, was also considered in the model. The formation of other complex oxides, such as $MnO.SiO_2$, $2MnO.SiO_2$, and $2SiO_2.3Al_2O_3$, was not considered in the present study. However, these oxides could easily be added to the model at a later stage. Various issues related to different stages of the inclusion model development are discussed in the sections below.

Equilibrium calculations for kinetic descriptions

When calculating thermodynamic equilibrium between liquid steel and inclusions, it is necessary to consider all the oxides, sulphides, and nitrides in liquid steel. The equilibrium at a particular temperature must be calculated with a minimum free energy criterion. This type of calculation will yield various fractions of oxides, sulphides, nitrides, and liquid steel, each with different compositions, and can be performed with thermodynamic software such as ThermoCalc.[14] However, the extension of such thermodynamic calculations to encompass kinetic constraints on the simultaneous formation of various phases needs to be developed.

During weld cooling, many phases (oxides, sulphides, and nitrides) can form simultaneously and the kinetics of one phase can interfere with the kinetics of the other phases. There are no established methods to consider such simultaneous reaction kinetics. Recent work has shown that simultaneous reaction kinetics can be handled with modified Johnson–Mehl–Avrami type equations.[17] However, parameters for this approach require experimental data, which are not available for reaction kinetics in liquid steel. Therefore, in the present inclusion model, the following assumptions were made.

At a particular temperature, the thermodynamic equilibrium between liquid steel and one phase only is considered at a particular time, ignoring the effects of other phases. With this assumption, the free energy of formation and equilibrium interface concentrations for the phase being considered can be calculated. The phases are assumed to be stoichiometric. The effects of all the alloying elements (C, Si, Mn, S, Cr, Mo, Ni, Al, Co, Cu, N, Ti, V, W, Zr, and O) to calculate the individual activities of each element. Therefore, the approach is consistent with multicomponent thermodynamic calculations between two phases. It is noteworthy that the present paper considers the reactions only in the liquid phase and does not take into account solidification, which will be dealt with in another paper. In a typical calculation of inclusion formation, liquid steel and Al_2O_3 equilibrium is calculated first. Then, the equilibrium between liquid steel and Ti_3O_5 is calculated. This is repeated for all the oxides and other phases such as AlN and MnS.

However, this approach introduces an ambiguity as far as selecting the phase that is first to form. To remove this ambiguity, the phase forming first is determined by the magnitude of the driving force for formation ΔG. For example, the driving force for an oxidation reaction represented by $x\underline{M} + y\underline{O} = M_xO_y$ is given by

$$\Delta G = \Delta G^0 + RT\ln(a_{M_xO_y}/a_{\underline{M}}^x a_{\underline{O}}^y) \quad \ldots\ldots\ldots (1)$$

where T is the temperature in kelvin, R is the gas constant, ΔG^0 is the standard free energy of oxide formation, $a_{M_xO_y}$ is the activity of the oxide, and $a_{\underline{M}}$ and $a_{\underline{O}}$ are the activities of the dissolved deoxidiser and oxygen respectively in the liquid steel. Further details can be found in Ref. 11. Similar equations are used for nitride and sulphide reactions. The first phase to form is the phase with the largest value for ΔG. Furthermore, the phase forming first is assumed to nucleate homogeneously.

Application of overall oxidation kinetics to continuous cooling

The extent of oxide formation at a particular temperature ζ can be estimated by using the overall reaction kinetics equation[11]

$$\zeta = 1 - \exp\{-[(c_{\underline{M}}^{i} - c_{\underline{M}}^{il})/(c_{\underline{M}}^{l} - c_{\underline{M}}^{il})]I^{vol}(8\pi/15)(\alpha_3^*)^3 t^{5/2}\} \quad \ldots\ldots\ldots (2)$$

where $c_{\underline{M}}^{i}$ and $c_{\underline{M}}^{il}$ are the equilibrium concentrations (in mole fraction) of the deoxidiser element in the inclusion and in the liquid at the liquid iron/inclusion interface respectively, $c_{\underline{M}}^{l}$ is the nominal concentration (in mole fraction) of deoxidiser in the liquid far away from the inclusion/liquid interface, $(c_{\underline{M}}^{l} - c_{\underline{M}}^{il})/(c_{\underline{M}}^{i} - c_{\underline{M}}^{il})$ is the equilibrium volume fraction of the considered oxide (for complex oxides such as $MnO.Al_2O_3$ it is assumed that the manganese flux matches the flux of aluminium, an assumption needed to simplify the multicomponent diffusion considerations and also the lack of diffusivity data for various elements in liquid steel), I^{vol} is the nucleation rate per unit volume, α_3^* is the parabolic thickening rate of the oxide, and t is the time of reaction at a particular temperature. The growth rate calculations assume a temperature independent, constant diffusivity for all of the elements in liquid steel. This is necessitated by the lack of experimental data on elemental diffusivity in liquid steel in the temperature range 2300–1800 K. Details of the calculation for nucleation rate and growth rate are given in Ref. 11, although the expressions are given below. The homogeneous nucleation rate (in some welding processes with metal transfer from electrodes insufficient melting may lead to injection of particles from the electrode which may act as heterogeneous nucleation sites) of an oxide in liquid iron I^{vol} can be calculated from

$$I^{vol} = A\exp(-\Delta G_{hom}^*/kT) \quad \ldots\ldots\ldots (3)$$

where ΔG_{hom}^* is the activation energy for the formation of the oxide nucleus, k is Boltzmann's constant, T is temperature in kelvin, and A is a pre-exponent factor. The value of A was assumed to be constant and equal to $10^{33}\ m^{-3}\ s^{-1}$.[11] The activation energy for nucleation of the oxide is given by

$$\Delta G_{hom}^* = (16\pi\sigma^3/3\Delta G_v^2) \quad \ldots\ldots\ldots (4)$$

where σ is the inclusion/liquid iron interfacial energy and ΔG_v is the free energy change per unit volume of the oxide ($= \Delta G/V_m$ where V_m is the molar volume of the oxide). In the following calculations the inclusion/liquid iron interfacial energy was assumed to be constant ($\sigma =$

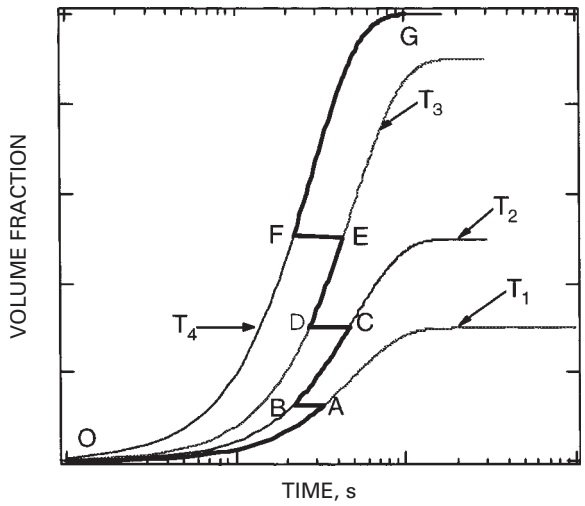

2 Schematic illustration of additive rule method used to calculate oxidation kinetics during continuous cooling

0·5 J m^{-2}). The parabolic thickening rate constant α_3^* is given by

$$\alpha_3^* = [2D_{\underline{M}}(c_{\underline{M}}^{l} - c_{\underline{M}}^{il})/(c_{\underline{M}}^{i} - c_{\underline{M}}^{il})]^{1/2} \quad . . . . . (5)$$

provided that $(c_{\underline{M}}^{l} - c_{\underline{M}}^{il})/(c_{\underline{M}}^{i} - c_{\underline{M}}^{il}) \ll 1$ and where $D_{\underline{M}}$ is the diffusivity of the deoxidiser (1×10^{-8} m^2 s^{-1}).

To model the reactions during continuous cooling, additivity of volume fractions is assumed and the calculations are modified accordingly. This calculation methodology is illustrated in Fig. 2, where the change in volume fraction of a particular oxide as a function of temperature T ($T_1 > T_2 > T_3 > T_4$) during continuous cooling is shown. The continuous cooling is broken into discrete time steps at discrete temperatures, T_1, T_2, T_3, and T_4. The extent of the isothermal reaction within time t_1 at temperature T_1 is calculated. Using equation (2), an equivalent reaction time at T_2 is determined and then the reaction is allowed to proceed isothermally for time t_2 at temperature T_2. This process is repeated as cooling continues. The overall reaction path during continuous cooling is shown by OA–BC–DE–FG in Fig. 2. This type of calculation is necessary because the maximum extent of reaction may be different at each temperature.

In this model, the completion of a particular reaction is determined by the extent of the reaction. Ideally, the extent of reaction should reach 1 for completion. However, equation (2) is not valid for the last stages of reaction when there is a diffusion field overlap. Therefore, the reaction is assumed to be complete once the extent of reaction reaches 0·9, i.e. as soon as ζ reaches 0·9, it is taken to be 1. Once the reaction is complete for a particular oxide at T_{final}, the residual liquid steel concentration for the deoxidiser element and oxygen is reset to the equilibrium concentration calculated at T_{final}. These calculations are repeated for the whole temperature range and the extent of formation of various oxides during weld cooling is evaluated. The accrued volume fraction of all the phases is taken as the final volume fraction V_f of inclusions. The relative compositions of the original and the final liquid allow an 'average' inclusion composition to be calculated.

Calculation of inclusion number density and size

The overall kinetic calculations described above consider the formation of individual phases during continuous cooling. To estimate the overall number density N_V of these phases the nucleation events of all the phases could simply be integrated. However, it is known that the later inclusions form by preferential heterogeneous nucleation on the oxides that have formed first during weld cooling.[11] As a result, pure phases such as Al_2O_3 and TiO_2 are not observed separately in the weld metal region. Therefore, the inclusion model needs to consider the heterogeneous nucleation of phases on the first formed oxide. This was achieved by equating the number density to the integrated nucleation rate of the first formed oxide

$$N_V = \sum_{T=T_{start}}^{T=T_{final}} I_T^{vol} \Delta t_T \quad . . . . . (6)$$

where I_T^{vol} is the homogeneous nucleation rate of the first forming oxide, Δt_T is the time spent at temperature T, T_{start} is the temperature at which the first oxide starts to form, and T_{final} is the temperature at which the extent of reaction reaches 0·9 for the first oxide. Once formation of the first oxide is complete, the final number density of inclusions is fixed by equation (6).

This particular step needs detailed discussion. Heterogeneous nucleation I_{het} is given by

$$I_{het} = B \exp(-\Delta G_{het}^*/kT) \quad . . . . . (7)$$

where B is the frequency factor and ΔG_{het}^* is the activation energy for heterogeneous nucleation. The value of ΔG_{het}^* is given by

$$\Delta G_{het}^* = \Delta G_{hom}^* f(\theta) \quad . . . . . (8)$$

where θ is the contact angle of the nucleus on the substrate on which nucleation occurs and $f(\theta)$ is given by

$$f(\theta) = (2 + \cos\theta)(1 - \cos\theta)^2/4 \quad . . . . . (9)$$

Since most of the information needed by equations (8) and (9) is not readily available, the present model takes $f(\theta) = 0$. This assumes complete wetting of phases that form later and the first forming oxide.[11] This reduces the heterogeneous nucleation rate so that it is equal to the frequency factor B in m^{-3} s^{-1}. The frequency factor should be related to the number of available nucleation sites, which is the integrated nucleation rate of the first forming oxide or N_V in m^{-3}, represented by

$$I_{het} = B = \eta N_V \quad . . . . . (10)$$

where η is the rate factor at which these nuclei become active and has dimensions s^{-1}. The choice of the value for η is rather arbitrary so it is assumed to be 1 s^{-1}. It is noteworthy that this value can be chosen such that I_{het} is high or low compared to the value of A used in equation (3). Therefore, the sensitivity of the calculations to this value was evaluated later and the value of 1 s^{-1} was found to be the most appropriate. In the subsequent calculations, the nucleation rate of all other oxides, sulphides, and nitrides is equated to I_{het}, given by equation (10).

This approach attempts to model heterogeneous nucleation on the surface of the first formed oxide. With an estimate of the number density N_V and the volume fraction of the average inclusions V_f, the average inclusion radius r_{inc} can be calculated using the relation

$$V_f = N_V(4/3)\pi(r_{inc})^3 \quad . . . . . (11)$$

Calculation of weld cooling curve

To calculate the overall kinetics during weld cooling, the inclusion model needs an estimate of the thermal cooling curve for the weld metal region in the temperature range 2300–1800 K. The analytical equation developed by Ion *et al.*,[18] which describes the temperature variation in a weld as a function of welding parameters, location in the transverse section (y, z), and time, is

$$T = T_0 + \left(\frac{q/v}{2\pi\lambda[t(t+t_0)]^{1/2}} \times \exp\left\{ -\frac{1}{4a}\left[\frac{(z+z_0)^2}{t} + \frac{y^2}{t+t_0} \right] \right\} \right) \quad . . . . (12)$$

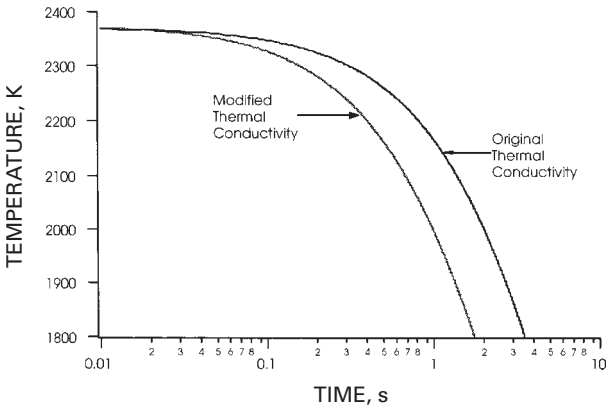

3 Comparison of weld metal cooling curves predicted by equation (12) with and without modified thermal diffusivity and using various parameters given in Table 1: welding parameters are voltage 30 V; current 450 A; speed $2{\cdot}6 \times 10^{-3}$ m s^{-1}; preheat temperature 293 K, yielding heat input 5·2 kJ mm^{-1}

where T_0 is the preheat temperature, q is the net heat input in joules, v is the welding velocity in m s^{-1}, λ is the thermal conductivity in J s^{-1} m^{-1} K^{-1}, t is the time in s, y is the distance along the width of the plate, z is the distance along the thickness of the plate, a is the thermal diffusivity in m^2 s^{-1}, and $t_0 = r_B^2/4a$ and $z_0 = [(r_B/e)(\pi a r_B/v)]^{1/2}$ where r_B is the radius of the heat source in m. Typical constants used for the inclusion cooling curve calculations are given in Table 1. It is known that the above equations do not consider the effect of convective heat transfer owing to fluid flow in the weld metal. The convective heat flow corresponds to an equivalent enhanced thermal conductivity of liquid steel. Therefore, in the present work, the λ value was enhanced by a factor of 2·25, chosen based on the work of Mundra *et al.*[19] Figure 3 compares the effect of using enhanced thermal conductivity on a typical weld cooling curve estimated by equation (12). The calculated weld cooling curves were then used with the overall oxidation kinetics model.

Weld cooling curve calculation with heat transfer and fluid flow model

Equation (12) considers only conductive heat transfer. The effect of convective heat transfer is considered by including an enhanced thermal conductivity. However, this may not be applicable in all welding conditions. Ideally, weld thermal history calculations that consider conductive and convective heat transfer more rigorously should be used. This would enable the inclusion model to be applied to a wide range of welding processes and welding parameters. As a preliminary evaluation, the inclusion model was coupled with a heat transfer and fluid flow model developed by

Table 1 Physical constants and assumed values for various parameters used in equation (12)*

Constants and variables	Value
Thermal conductivity of iron λ	41·0 J s^{-1} m^{-1} K^{-1}
Volume thermal capacity ρC	$4{\cdot}5 \times 10^6$ J m^{-3} K^{-1}
Thermal diffusivity $a = \lambda/\rho C$	$9{\cdot}0 \times 10^{-6}$ m^2 s^{-1}
Radius of heat source r_B	1×10^{-3} m
Location† y, z	20×10^{-6} m

* Other welding parameters such as q, v, and T_0 are user input to the equation.
† Location chosen such that the peak temperature at this location exceeds 2300 K, the dissolution temperature of Al_2O_3.

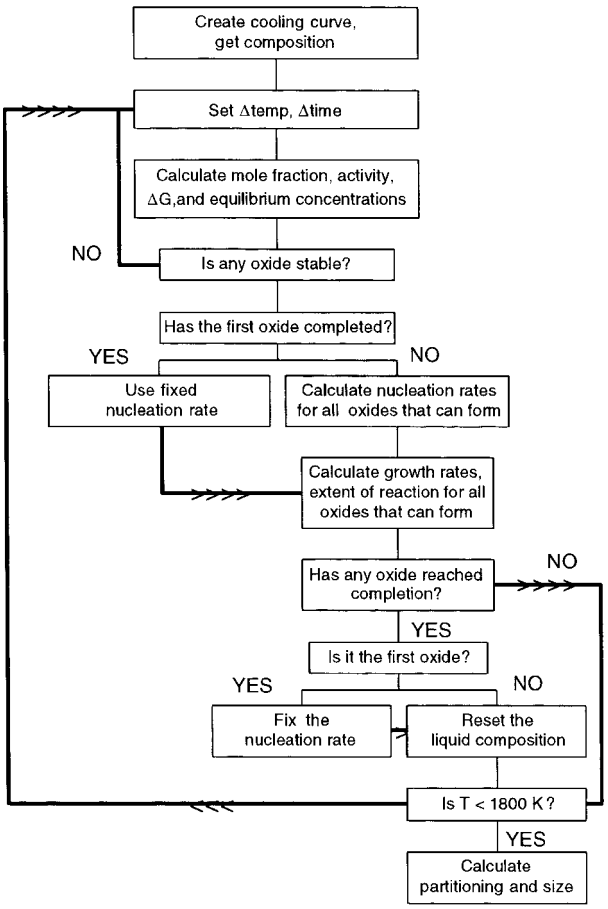

4 Flow chart of integrated inclusion model showing calculation steps

Mundra *et al.*[19] for a few conditions. Specimen geometry, thermophysical parameters, weld metal composition, and welding process parameters are given as inputs to the numerical heat transfer and fluid flow model, which calculates thermal cycles. Calculated thermal cycles and the weld metal composition are taken as the inputs to the inclusion model and the inclusion characteristics are calculated.

Integrated inclusion model with weld cooling curves

The calculation steps in the overall inclusion model are shown in Fig. 4. The calculation starts with the creation of a cooling curve as a function of welding process parameters using equation (12) or with the heat transfer and fluid flow model. Weld metal composition is then added as input to the model. Calculations are started at 2300 K. At this temperature, for most of the low alloy steels, only the liquid phase is stable. At each temperature step, the calculations evaluate the mole fraction and activity of dissolved elements in the liquid steel as well as the free energy of formation and equilibrium concentrations for various liquid steel–oxide, liquid steel–AlN, and liquid steel–MnS reactions. Based on the ΔG values, the type of oxide, sulphide, or nitride that forms can be deduced. The nucleation rate, growth rate, and extent of reaction for each phase are calculated. This was repeated for each temperature step until the extent of a particular oxide reaction reached 0·9. Once this condition is satisfied for the first forming phase, the final inclusion number density is set to the integrated nucleation rate of the first forming phase, as mentioned above. Moreover, the liquid steel concentrations are reset to new levels accounting for the completion of this first oxide reaction. With the reduction in temperature, the

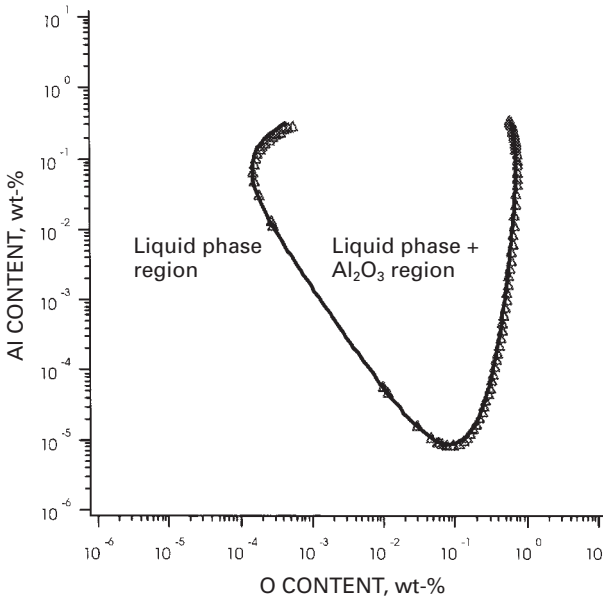

△ ThermoCalc; —— present work

5 Comparison of calculated phase boundary between liquid steel and Al_2O_3 in Fe–Al–O ternary system at 1800 K obtained from present inclusion model with that from ThermoCalc[14]

extent of reaction of other phases is calculated, with the heterogeneous nucleation condition as described above. As other reactions are completed, the liquid concentrations are reset to new levels. All the reactions during cooling are recorded during calculations. Once the temperature reaches 1800 K, the calculations are stopped and inclusion characteristics summarised.

RESULTS AND DISCUSSION

Application of inclusion model

As a first step, the reliability of calculating the equilibrium between liquid steel and various oxides was evaluated. Figure 5 compares the calculated phase boundary between liquid steel and Al_2O_3 in the Fe–Al–O system at 1800 K determined by the equilibrium thermodynamic description in the present inclusion model with ThermoCalc.[14] The calculations agree well with each other and establish confidence in the present inclusion model.

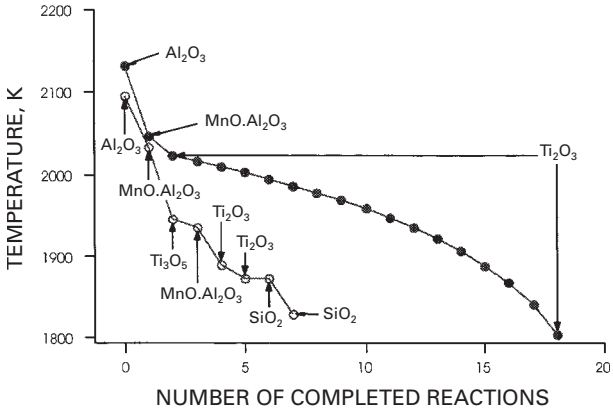

○ C1; ● C9

6 Predicted progression of reaction for weld compositions C1 and C9 in Table 2

As in the earlier work,[11,12] the inclusion model was applied to the experimental results of Kluken and Grong.[7] The experimental compositions examined are given in Table 2. Weld cooling curves were calculated using equation (12) (*see* Fig. 3). Representative oxidation sequences for two welds, C1 and C9, are compared in Fig. 6, which shows the temperatures at which various oxide reactions were completed, i.e. when $\zeta = 0{\cdot}9$. Duplicate points, such as those for Ti_2O_3 in C9, indicate that formation of Ti_2O_3 was completed at a given temperature ($\zeta = 0{\cdot}9$) and that additional Ti_2O_3 formed later as temperature dropped and the composition changed following completion of the earlier inclusion formation. In all welds Al_2O_3 was the first forming oxide. Figure 6 shows that Ti_2O_3 forms over a wider range of temperatures in weld C9 compared with weld C1. This is obviously a result of the high titanium concentration in the C9 weld. However, Ti_3O_5 did not form in weld C9. Although the silicon concentration is higher in C9 than in C1, the calculations showed an absence of SiO_2 formation in C9 while it did form in C1. The above results can be traced to the relative phase stability between oxides and show that the inclusion model is quite sensitive to weld metal composition, which is reflected in the oxidation sequence.

For all of the welds, the inclusion model did not predict the formation of MnS or AlN. This is attributed to insufficient supersaturation of sulphur and nitrogen in the

Table 2 Weld metal compositions of submerged arc welds*: after Kluken and Grong,[7] wt-%

	Alloy								
Element	C1	C2	C3	C4	C5	C6	C7	C8	C9
C	0·09	0·09	0·1	0·1	0·09	0·09	0·09	0·1	0·09
Si	0·48	0·55	0·69	0·52	0·58	0·69	0·53	0·62	0·62
Mn	1·86	1·84	1·88	1·87	1·95	1·97	1·9	1·92	1·78
S	0·01	0·01	0·01	0·007	0·009	0·009	0·008	0·01	0·007
Cr	0	0	0	0	0	0	0	0	0
Mo	0	0	0	0	0	0	0	0	0
Ni	0·05	0·07	0·06	0·08	0·06	0·06	0·09	0·07	0·07
Al	0·018	0·02	0·028	0·041	0·037	0·044	0·062	0·062	0·053
Co	0	0	0	0	0	0	0	0	0
Cu	0·02	0·03	0·03	0·06	0·03	0·03	0·03	0·03	0·08
N	0·005	0·005	0·008	0·005	0·005	0·006	0·005	0·005	0·006
Ti	0·005	0·025	0·063	0·005	0·022	0·058	0·008	0·032	0·053
V	0·02	0·02	0·02	0·01	0·02	0·02	0·02	0·02	0·01
W	0	0	0	0	0	0	0	0	0
Zr	0	0	0	0	0	0	0	0	0
O	0·034	0·037	0·035	0·03	0·039	0·04	0·032	0·031	0·031
Fe	Bal.	Bal.	Bal.	Bal.	Bal.	Bal.	Bal.	Bal.	Bal.

* Welding parameters: voltage 30 V, current 450 A, speed $2{\cdot}6 \times 10^{-3}$ m s^{-1}.

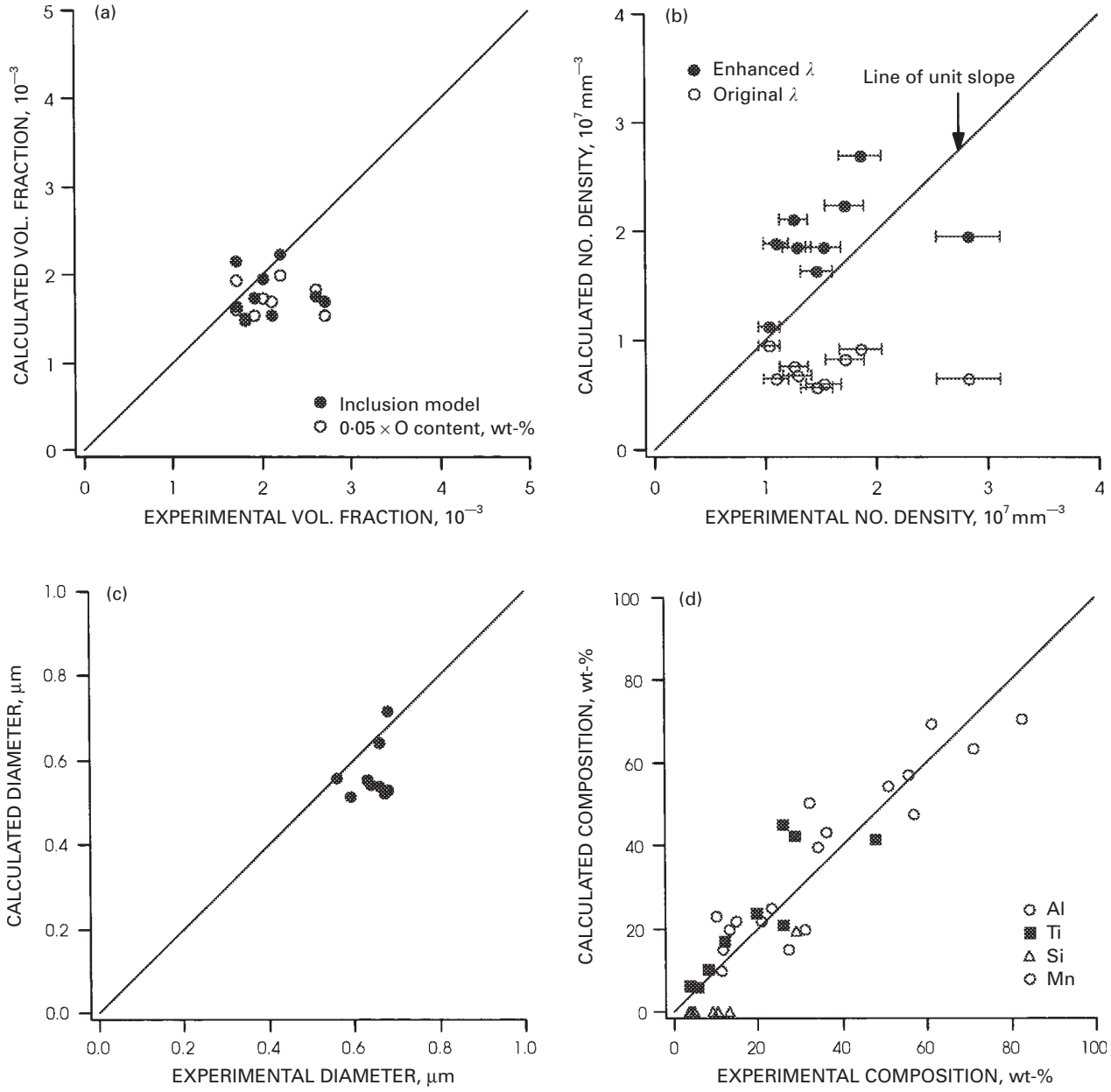

a volume fraction estimations from inclusion model and empirical relation; *b* number density, showing calculations with original and enhanced (2·25λ) thermal conductivity; *c* inclusion diameter; *d* inclusion composition

7 Comparison of predicted and measured data from Ref. 7

liquid steel. By increasing the concentration of sulphur and nitrogen, these compounds can be forced to form at low temperatures. The supersaturation of these elements in the liquid steel may also be enhanced by partitioning during solidification of ferrite, which is not considered in the present work.

The calculated inclusion characteristics, volume fraction, number density, diameter, and inclusion composition, for the welds are compared with the experimental data in Fig. 7. The volume fraction of inclusions (Fig. 7*a*) compare fairly well with the experimental data. Traditionally, the volume fraction of inclusions was estimated as a function of oxygen concentration based on extensive data ($V_f \simeq 0{\cdot}05$ wt-%O).[20] These estimates are also shown in Fig. 7*a*. The predictions of both methods are comparable, which shows the validity of the inclusion model for estimating the volume fraction of inclusions.

Values of calculated number density of inclusions N_V are compared with experimental data in Fig. 7*b*. The error bars correspond to $\pm 10\%$ error in the experimental measurements. The number density estimations depend strongly on the weld cooling rate. Variation in N_V for the welds with two different weld cooling curves (*see* Fig. 3) is compared. The calculated N_V values for the weld cooling curve with the original thermal conductivity were found to be lower than those for the weld cooling curve with the modified thermal conductivity. The enhanced thermal conductivity λ predicts values in closer agreement with the experimental measurements and therefore using an enhanced λ value seems to be a useful means of compensating for thermal convection that is not considered in the analytical expression. Given the approximate nature of the analytical expression for the weld cooling curve, the predictive capability of the model seems fair.

Since the first forming oxide in all the welds was Al_2O_3, the number density calculation is related to the nucleation rate of Al_2O_3. For example, even with a high titanium concentration, the first forming oxide in the C9 weld was Al_2O_3. Therefore, for a given concentration of aluminium and oxygen, the variation of titanium concentration may

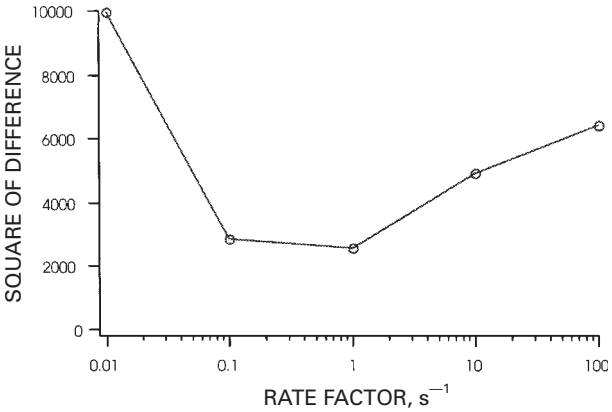

8 Variation of calculated square of difference between predicted and experimental inclusion composition with rate factor in equation (10): plot shows rate factor of 1 gives lowest error

not induce large changes in N_V since it will be controlled by the Al_2O_3 nucleation rate. The calculated inclusion diameters also compare fairly well with experimental data (Fig. 7*c*). The diameter estimations are directly linked to the number density and volume fraction calculations as discussed above. Therefore, the accuracies of the estimations are all interrelated.

The calculated inclusion compositions (i.e. the concentrations of aluminium, titanium, silicon, and manganese) are compared with the experimental data from Ref. 7 in Fig. 7*d*. The plot again shows a fair correlation. For all cases, the manganese contribution to inclusions is a result of the formation of $MnO.Al_2O_3$. The calculations indicate no MnO formation. In many cases, the calculated silicon concentrations in the inclusions were zero. This is attributed to the inability of the inclusion model to consider the formation of complex $MnO.SiO_2$ (rhodonite) during solidification.

Analysis of model calculations showed that the inclusion compositions were sensitive to the assumed value for the rate factor η ($= 1\ s^{-1}$) of heterogeneous nucleation on the first forming oxide. Therefore, a sensitivity analysis was carried out to estimate the errors in the composition estimation for different rate factors (ranging from 0·01 to 100). The calculations showed that if the rate factor is low (e.g. 0·01), the inclusion composition is rich in aluminium and titanium, indicating the predominant presence of Al_2O_3 and Ti_xO_y type oxides. However, if the rate factor is high (e.g. 100), the concentration of manganese and silicon increased, indicating the promotion of low temperature oxides such as SiO_2 and MnO. This is an expected result because having a low value of η decreases the oxidation kinetics of low temperature oxides such as MnO and SiO_2. In contrast, a large η value promotes the kinetics of low temperature oxides. However, to choose a rate factor value for further calculations, it is necessary to compare the errors of prediction (i.e. (experimental composition − predicted composition)^2) with different rate factors. This comparison is shown in Fig. 8, which indicates that the errors are minimal when the rate factor is taken as $1\ s^{-1}$.

The calculated residual concentrations of aluminium and titanium in the liquid (which ends up as solid solution in the matrix) at the end of the deoxidation reaction are compared with experimental data from Kluken[21] in Fig. 9. Both calculations and experimental values show an increase in residual concentrations with an increase in the bulk concentration in the weld. Although the calculations do not match the experimental values, the expected trends (increase of concentration in solution with increase of concentration in weld) can be seen. However, the calculations show

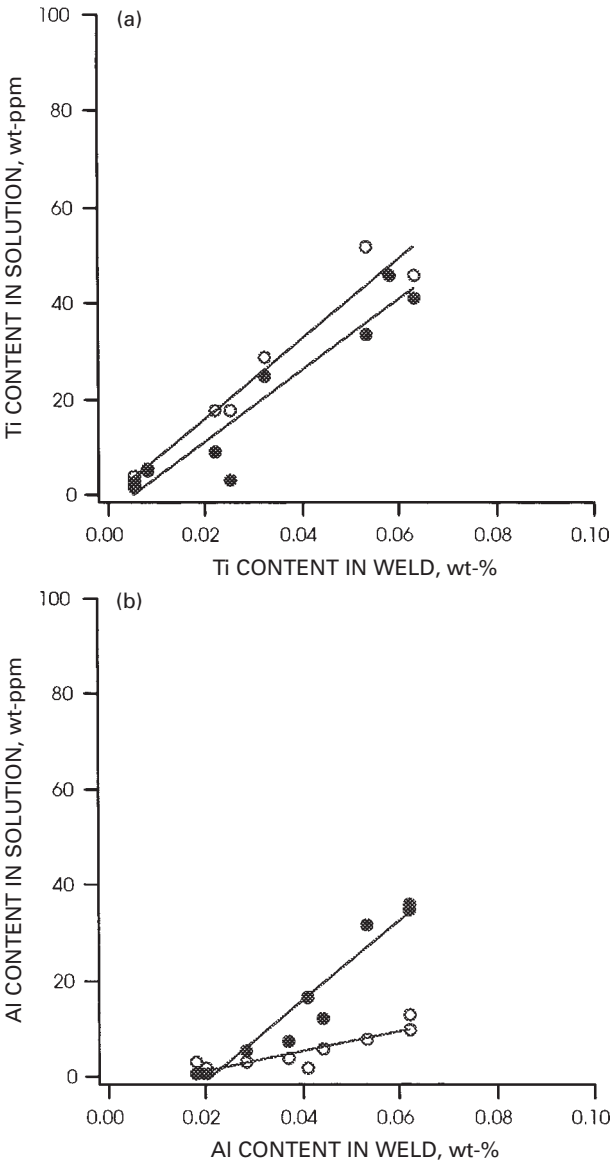

○ experimental; ● calculated
a of Ti in solid solution; *b* of Al in solid solution

9 Comparison of predicted and experimental residual concentration

an overprediction of aluminium in solution and a fair correlation with titanium in solution. This suggests that in the experimental welds of Kluken, excessive formation of Al_2O_3 had occurred in comparison with the calculated values. However, the present calculations of aluminium concentration in the actual inclusions seem to show fair correlation (Fig. 7*d*) with the measured values. This discrepancy may be related to the precipitation of AlN. The amount of aluminium in solution will decrease with AlN formation during solidification and during subsequent weld cooling in the solid state. The capability to calculate the aluminium and titanium in solid solution is critical for evaluating their effect on the solid state decomposition of austenite to ferrite.

Coupled heat transfer, fluid flow, and inclusion model

To test the coupled heat transfer, fluid flow, and inclusion model, the cooling curves for welds in Table 3 were calculated using the numerical heat transfer and fluid flow model.[19] The coupled model was used to evaluate the sensitivity of the predictions to the variations in heat input

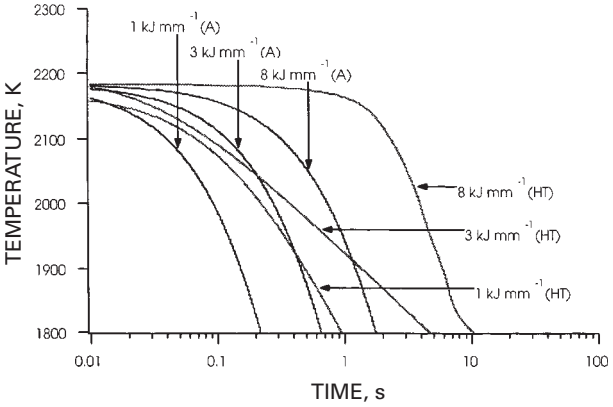

HT: predicted by heat transfer and fluid flow model of Mundra *et al.*;[19] A: predicted by analytical model with enhanced thermal conductivity

10 Weld cooling curves for submerged arc welds with three heat input values

(1–8 kJ mm^{-1}). The weld cooling curves predicted by the heat transfer and fluid flow model are shown in Fig. 10. The plot also shows the predicted weld cooling curves from the analytical model (equation (12)). The cooling rate values from the analytical equation were found to be larger than those of the heat transfer and fluid flow model. However, both methods show the expected increase in cooling rate with a decrease in the heat input. The variation of predicted inclusion number density and diameter are compared with the experimental data in Fig. 11, which shows agreement with the experimental trends. Inclusion diameter increased with an increase in weld heat input and inclusion number density increased with a decrease in weld heat input. The experimental weld compositions (Table 3) in this analysis are more or less similar. Therefore, the increase in the number density of inclusions with low weld heat input is mainly a result of the increase in the cooling rate. Rapid cooling conditions force the first forming oxide to form at much lower temperatures than under slow cooling conditions. Since the nucleation rate increases exponentially with decreasing temperature, an increase in inclusion

Table 3 Weld metal compositions and welding parameters of submerged arc welds (series 4) with varying welding heat input: after Kluken and Grong[7]

	C18	C19	C20
Content, wt-%			
C	0·09	0·08	0·08
Si	0·7	0·77	0·75
Mn	1·89	1·96	1·91
S	0·006	0·005	0·006
Cr	0	0	0
Mo	0	0	0
Ni	0·1	0·06	0·08
Al	0·028	0·023	0·026
Co	0	0	0
Cu	0	0·03	0·04
N	0·006	0·006	0·007
Ti	0·058	0·043	0·046
V	0·02	0·02	0·02
W	0	0	0
Zr	0	0	0
O	0·022	0·03	0·029
Fe	Bal.	Bal.	Bal.
Voltage, V	30	30	30
Current, A	800	400	300
Speed, mm s^{-1}	3	4	9
Heat input, kJ mm^{-1}	8	3	1

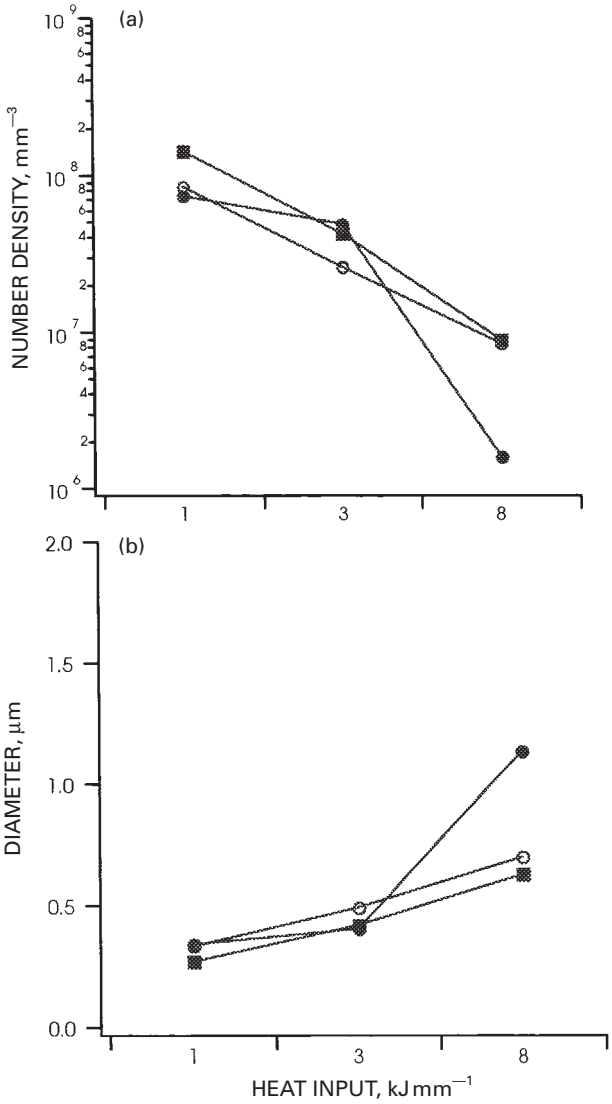

○ experimental; ● heat transfer and fluid flow model; ■ analytical weld cooling curve model
a inclusion number density; *b* diameter

11 Comparison of given parameters from coupled heat transfer, fluid flow, and inclusion model with experimental measurements from Refs. 7 and 21

number density is found for rapid cooling conditions. Moreover, the plot also shows that the predicted inclusion characteristics from the analytical equations are better than those from the heat transfer and fluid flow model. At first, this result dispels the need for sophisticated heat transfer and fluid flow models to estimate the weld cooling curve. Although this may be valid for the heat input levels used in the present work, other recent work has shown that the analytical equations do not give satisfactory predictions of inclusion characteristics. The discrepancy was found for rapid cooling conditions in laser and electron beam welds.[16] Therefore, further work is needed to evaluate the coupled heat transfer, fluid flow, and inclusion model over a wide range of welding conditions and processes.

Although the results of the inclusion model compare fairly well with the experimental measurements, the model needs further improvements. First, the inclusion model presently does not consider the effects of collision and coalescence of inclusions in the liquid weld metal. Recent work by Babu *et al.*[22] has shown that, in the presence of fluid flow gradients and large residence times, the inclusions can collide with each other and may coarsen rapidly. This

needs to be incorporated into the model. Second, the inclusion model considers monotonic cooling at a given location in the weld. This is because the model has an inherent assumption of stationary inclusions in the presence of fluid flow in the weld. It is well known that weld fluid flow conditions transport mass from low temperature regions to high temperature regions. This mass transport will also induce movement of inclusions. Therefore, it is highly unlikely that these inclusions will experience monotonic cooling conditions. Recent work by Pitscheneder *et al.*[23] using a particle tracking approach has shown that an inclusion may experience complex thermal cycles of heating and cooling owing to its movement in the molten pool. This was shown to result in cyclic formation and dissolution of Al_2O_3 inclusions. This particle tracking approach should be incorporated into a generalised, coupled heat transfer, fluid flow, and inclusion model to study the effects of weld process parameters. Third, in addition, complex oxides and liquid slag formation need to be considered and, fourth, the coupled model also needs to incorporate partitioning effects caused by ferrite solidification ($T < 1800$ K) on inclusion formation. Ferrite solidification partitioning will be influenced by weld cooling rate and weld metal composition. Modelling efforts to consider the solidification are being pursued with thermodynamic calculations and using Clyne–Kurz approximations,[24] similar to the approach by Matsumiya *et al.*[25]

CONCLUSIONS

A model based on thermodynamics and overall oxidation kinetics has been developed to describe inclusion formation in liquid steel for low alloy steel welds. The model considers the effect of weld metal composition and the weld cooling rate on the overall oxidation kinetics of various oxides. Calculations of the inclusion model, coupled with analytical weld cooling curve predictions, compared fairly well with experimental data. The model showed the close relationship between overall weld metal composition and the oxidation sequence during weld cooling.

The present work also showed the importance of weld cooling curve calculations in the prediction of values of inclusion characteristics. Preliminary work on the coupled heat transfer, fluid flow, and inclusion model was able to predict the variation of inclusion size and number density as a function of weld heat input in submerged arc welds. The predicted values are similar to that predicted by the analytical model and agree with experimental trends.

The model needs to be evaluated over a wide range of welding heat input conditions in manual metal arc welding, flux cored arc welding, and submerged arc welding processes. Moreover, the model needs to be applied to other welding processes such as laser, electron beam, and electroslag processes. However, advanced thermal models are needed to describe the thermal excursions in the weld metal region. These models need to be extended to consider collision and coalescence of inclusions, spatial gyrations, and solidification conditions.

ACKNOWLEDGEMENTS

This research was sponsored by the Division of Materials Sciences, US Department of Energy, under contract DE–AC05–96OR22464 with Lockheed Martin Energy Research Corp. The authors would like to thank Alloy Rods Inc., Hanover, PA, USA for supplying the welds used in the present investigation. The authors would also like to thank Dr B. Radhakrishnan and Dr Q. Han of ORNL for helpful comments on the present paper.

REFERENCES

1. G. M. EVANS and N. BAILEY: 'Metallurgy of basic weld metal'; 1997, Cambridge, Abington Publishing.
2. Y. ITO and M. NAKANISHI: *Sumitomo Search*, 1976, **15**, 42–62.
3. D. J. ABSON and R. J. PARGETER: *Int. Met. Rev.*, 1986, **31**, (4), 141–194.
4. Ø. GRONG and D. K. MATLOCK: *Int. Met. Rev.*, 1986, **31**, (1), 27–48.
5. H. K. D. H. BHADESHIA: 'Bainite in steels'; 1992, London, The Institute of Materials.
6. F. ISHIKAWA, T. TAKAHASHI, and T. OCHI: *Metall. Trans. A*, 1994, **25A**, 929–936.
7. A. KLUKEN and Ø. GRONG: *Metall. Trans. A*, 1989, **20**, 1335–1349.
8. N. BAILEY and R. J. PARGETER: 'The influence of flux type on the strength and toughness of submerged arc weld metal', 33–80; 1988, Cambridge, The Welding Institute.
9. F. C. LIAO and S. LIU: *Weld. J.*, 1992, **71**, 94s–103s.
10. H. K. D. H. BHADESHIA and L.-E. SVENSSON: 'Mathematical modelling of weld phenomena', (ed. H. Cerjak and K. E. Easterling), 109–180; 1993, London, The Institute of Materials.
11. S. S. BABU, S. A. DAVID, J. M. VITEK, K. MUNDRA, and T. DebROY: *Mater. Sci. Technol.*, 1995, **11**, (2), 186–199.
12. S. S. BABU, S. A. DAVID, J. M. VITEK, K. MUNDRA, and T. DebROY: Proc. 4th Int. Conf. on Trends in Welding Research, (ed. H. B. Smartt *et al.*), 135–140; 1995, Materials Park, OH, ASM International.
13. K. C. HSIEH, S. S. BABU, J. M. VITEK, and S. A. DAVID: *Mater. Sci. Eng. A*, 1996, **A215**, 84–91.
14. B. SUNDMAN, B. JANSSON, and J.-O. ANDERSSON: *Calphad*, 1985, **9**, 153–190.
15. T. KOSEKI, S. OHKITA, and N. YURIOKA: *Sci. Technol. Weld. Joining*, 1997, **2**, (2), 65–69.
16. S. S. BABU, F. REIDENBACH, S. A. DAVID, T. BÖLLINGHAUS, and H. HOFFMEISTER: *Sci. Technol. Weld. Joining*, 1999, **4**, (2), 63–73.
17. S. J. JONES and H. K. D. H. BHADESHIA: *Acta Metall.*, 1997, **45**, 2911–2920.
18. J. C. ION, K. E. EASTERLING, and M. F. ASHBY: *Acta Metall.*, 1984, **32**, 1949–1962.
19. K. MUNDRA, T. DebROY, S. S. BABU, and S. A. DAVID: *Weld. J.*, 1997, **76**, 163s–171s.
20. A. G. FRANKLIN: *J. Iron Steel Inst.*, 1969, **207**, (2), 181–186.
21. A. KLUKEN: 'Modeling of reaction sequence during deoxidation and solidification of steel welds metal', PhD thesis, University of Trondheim, Trondheim, Norway, 1990.
22. S. S. BABU, S. A. DAVID, and T. DebROY: *Sci. Technol. Weld. Joining*, 1996, **1**, 17–27.
23. W. PITSCHENEDER, R. EBNER, T. HONG, T. DebROY, K. MUNDRA, and R. BENES: in 'Mathematical modelling of weld phenomena 4', (ed. H. Cerjak and H. K. D. H. Bhadeshia), 3–25; 1998, London, The Institute of Materials.
24. S. S. BABU, J. M. VITEK, S. A. DAVID, K. MUNDRA, and T. DebROY: Proc. 77th AWS Convention, Chicago, IL, USA, April 1996, AWS, 59–60 (abstract).
25. T. MATSUMIYA, T. KOSEKI, W. YAMADA, and Y. UESHIMA: *Nippon Steel Tech. Rep.*, 1993, **57**, 50–56.